Check for updates

Formation and Tuning of 2D Electron Gas in Perovskite Heterostructures

Igor V. Maznichenko,* Sergey Ostanin, Arthur Ernst, Juergen Henk, and Ingrid Mertig

Oxide interfaces provide very intriguing phenomena, in particular a 2D electron gas (2DEG) emerging between robustly insulating perovskites. The 2DEG was detected in 2004 beneath polar LaAlO$_3$ (LAO) epitaxially grown on TiO$_2$-terminated SrTiO$_3$ (001) (STO). Herein, recent first-principles studies of 2DEGs are reviewed. Using a Green function method, the family of the polar/nonpolar (001) interfaces: LAO/STO, LaFeO$_3$/STO, and STO/KTaO$_3$ is computed. In the context of 2DEG, one of two insulating perovskites, at least, must be polar. The effect of a polar/polar interface is modeled for LAO/KTaO$_3$(001) and also for the (110) and (111) interfaces of LAO/STO. Starting from the defectless superlattice with its two differently terminated interfaces, we demonstrate that the 2DEG and 2D hole gas appear there, respectively, due to the presence of excessive electrons or holes. 2DEG is evaluated by its layer-resolved density profile along [001], as well as the Fermi surface cross sections and effective masses, which are directly related to the transport properties. The effects of intermixed cations, their vacancies, and oxygen vacancies at each interface of LAO/STO are calculated. Finally, we show how to tune reversibly the 2DEG by changing the electronic balance at the LAO surface that mimics the effect of ionic liquid gating.

1. Introduction

The 2D electron gas (2DEG) emerging at the interface between robustly insulating perovskites, such as epitaxial LaAlO$_3$ (LAO) grown on SrTiO$_3$(001) (STO), is a prospective phenomenon that has motivated research since its discovery in 2004.[1–4]

Dr. I. V. Maznichenko, Dr. S. Ostanin, Dr. J. Henk, Prof. I. Mertig
Institute of Physics
Martin Luther University Halle-Wittenberg
D-06099 Halle (Saale), Germany
E-mail: igor.maznichenko@physik.uni-halle.de

Prof. A. Ernst
Institute of Theoretical Physics
Johannes Kepler University
A-4040 Linz, Austria

Prof. A. Ernst
Max Planck Institute of Microstructure Physics
Weinberg 2, D-06120 Halle (Saale), Germany

The ORCID identification number(s) for the author(s) of this article can be found under https://doi.org/10.1002/pssb.201900540.

Its mobility, for instance, is one order of magnitude higher than that of silicon-based transistors. The properties of this 2DEG are well understood.[5] The 2DEG can be detected with side electrodes or by tunneling measurements between the electron gas and metallic electrodes on LAO.[6]

It turned out that at least one of two insulating perovskites must be polar or ferroelectric.[7] LAO(001), for instance, represents alternately charged planes [LaO]$^+$ and [AlO$_2$]$^-$. Thus, each La atom at the TiO$_2$/LaO-terminated LAO/STO interface transfers half of an electron into the next and formally neutral TiO$_2$ layer of STO, thereby decreasing the oxidation state of the interfacial Ti atoms.[8–11]

Apart from LAO/STO, there is a family of composite perovskites for which the TiO$_2$/LaO termination appears unavoidably. For instance, 2DEG formation has been recently reported for STO(001) and epitaxially grown LaFeO$_3$ (LFO).[12] In addition, Li et al.[13] found that both crystalline and partially amorphous ABO$_3$/STO (A = La, Pr, Nd and B = Al, Ga) interfaces become conducting if the polar ABO$_3$ film is thicker than four unit cells (u.c.). This critical thickness has been established for the polar side of LAO/STO as well.[5,14]

So far, a limited number of experiments focused on tuning the buried interfacial 2DEG.[15,16] As perovskites grow in complete unit cells on atomically clean and TiO$_2$-terminated STO(001),[17] the LAO(001) surface is in any case AlO$_2$ terminated. There are two options to modify the electronic balance of this AlO$_2$ termination: either by capping layers or by liquid gating at the surface. The widely used capping is realized in LAO/STO heterostructures. However, this capped system excludes practically the scenario of a switchable 2DEG, whereas liquid gating may allow us to do that. Electrolyte gating is commonly used for accumulating relatively large carrier densities at oxide surfaces.[18]

In the case of LAO/STO, the extremely high mobility of the 2DEG of up to 10^4 cm^2 V^{-1}s^{-1} is realized by an ionic liquid-assisted field effect.[19] Most importantly, by changing the gate polarity and gate voltage, the controlled depletion of negatively/positively charged carriers can be achieved, which, in principle, will allow us to vary the 2DEG's conductivity from its large value down to zero. This is understood in terms of oxygen migration. With the use of the proper gate geometry and polarity, some of the oxygen vacancies distributed in LAO and interfacial vacancies can be filled. Then, by switching the gate polarity the O^{2-} ions can be partially pulled out from the LAO overlayers that make

up their composition and also the composition of the buried oxygen-deficient interface. Although the gate switching has not been shown to be completely reversible, its utilization allows the exploration of the effect of electrolytic gating on the 2DEG through measurements of electrical transport, X-ray absorption spectroscopy, and photoluminescence spectra.[19–24] The controlled formation of 2DEG via ionic liquid gating has been shown recently for the LaFeO$_3$/STO interface.[12]

All epitaxially grown composite perovskites contain intrinsic oxygen vacancies and intermixed cations near the interfaces.[25,26] Interfacial defects may induce additional charge carriers. Oxygen vacancies enhance the n-type doping[27] whereas the La/Sr interfacial mixing[28] may suppress the 2DEG. Experimentally, LAO/STO interfaces prepared at 500 °C and below become insulating after oxygen annealing (when the O redox mechanism is removed), whereas samples prepared at 515 °C and above are conducting.[13] In intrinsically imperfect LAO, therefore, vacancy filling may be controlled by the growth temperature.

Density functional theory (DFT) calculations suggest that the significant reconstruction near the TiO$_2$/LaO interface compensates for the dipolar electric field in the LAO overlayers.[29] The 2DEG scenario based on the Ti$^{3.5+}$ valence state can be successfully simulated from first principles.[5,30] Over the past decade, the LAO/STO structural model transformed from superlattices[31,32] to slab geometries with a vacuum region.[27,30,33–39] Meanwhile, the 2DEG mechanism of interfacial oxygen vacancies, combined with the Hubbard parameterization of the 3d states of interfacial Ti, has been used as well.[40] All these theoretical efforts have been made to improve on the computed 2DEGs. Nevertheless, the asymmetrical superlattice with its two interfaces remains a good starting point for 2DEG studies. Previously published DFT calculations show the nonzero density of states at the SrO/AlO$_2$ interface that means the presence of 2D hole gas (2DHG) there.[29,31,41] Recent *ab initio* calculations of the LAO/STO superlattice within a Green function (GF) method[42,43] show that the 2DEG and 2DHG could be suppressed by additional doping with opposite charge.[44]

In this work, we compare our ab initio results obtained within a superlattice approach for various polar/nonpolar interfaces: LAO/STO(001), LFO/STO(001), and STO/KTaO$_3$(001); basics of the computations can be found in the preceding article of this issue and details elsewhere.[12,44,45] We discuss in particular how the interfacial band bending affects the 2DEG carrier densities. In addition to the polar/polar interfaces of LAO/KTaO$_3$(001) we discuss the (110) and (111) interfaces of LAO/STO, at which the STO layers are polar. To study the 2DEG variations arising due to interfacial defects, we simulate various kinds of long-range disorders such as oxygen vacancies, cation vacancies, and their intermixing across both interfaces of the LAO/STO(001) superlattice. The coherent potential approximation (CPA) offers an elegant way to describe O vacancies and cation substitutes in the framework of a self-consistent GF formalism[46] that adequately describes the LAO/STO interfaces.[44]

The tuning of buried 2DEG is investigated by evaluating its density from the Fermi surface cross sections and effective masses of electrons, both of which are directly related to various transport properties. The scenario of a switchable 2DEG is exemplified by AlO$_2$-terminated LAO/STO(001), calculated within a slab geometry and CPA. This may disclose the conditions at

Igor V. Maznichenko studied physics at Rostov State University (currently in Southern Federal University) in Russia until 2000. He received a DAAD scholarship for a research visit at the Martin Luther University Halle-Wittenberg in 2002–2003. He obtained his Ph.D. from Rostov State University in 2004. Since 2005, he is a researcher at the Martin Luther University Halle-Wittenberg. He has been a postdoctoral fellow in the CRC 762 "Functionality of Oxide Interfaces" since 2008 until 2019.

Juergen Henk obtained his Ph.D. from the University of Kiel in 1991 and his *venia legendi* (postdoctoral lecture qualification, "Habilitation") from the Martin Luther University Halle-Wittenberg in 2005. He was a postdoctoral fellow at the universities of Duisburg-Essen (Germany) and Uppsala (Sweden). From 1999 until 2011, he was a staff scientist at the Max Planck Institute of Microstructure Physics in Halle. Since 2012, he holds a permanent position as a staff scientist at the Martin Luther University Halle-Wittenberg.

Ingrid Mertig obtained her Ph.D. from TU Dresden in 1982. She was a DFG Heisenberg Fellow from 1997 to 2001. Since 2001, she is a full professor for physics at the Martin Luther University Halle-Wittenberg. She was a Max Planck Fellow from 2006 to 2018. She held guest professorships at the New York University, the University Paris-Sud, the University of Nagoya, and at Bristol University. She was the spokesperson of the CRC 762 "Functionality of Oxide Interfaces" (2008–2019). From 2011–2017 she was a member of the German Council of Science and Humanities.

the LAO surface needed to vary the buried 2DEG. On top of this, we mimic liquid gating, thereby simulating its effect on the 2DEG from first principles.

2. Ideal Superlattices

2.1. Polar/Nonpolar Interface

2.1.1. LaAlO$_3$/SrTiO$_3$(001)

The local electronic structures of stoichiometrically perfect and dually terminated LAO/STO(001) have been computed for superlattices constructed from cubic STO and LAO (we choose the experimental lattice parameter of bulk STO also for LAO). The energy positions of the valence band maximum and the conduction band minimum yield band-edge profiles for the [001] direction
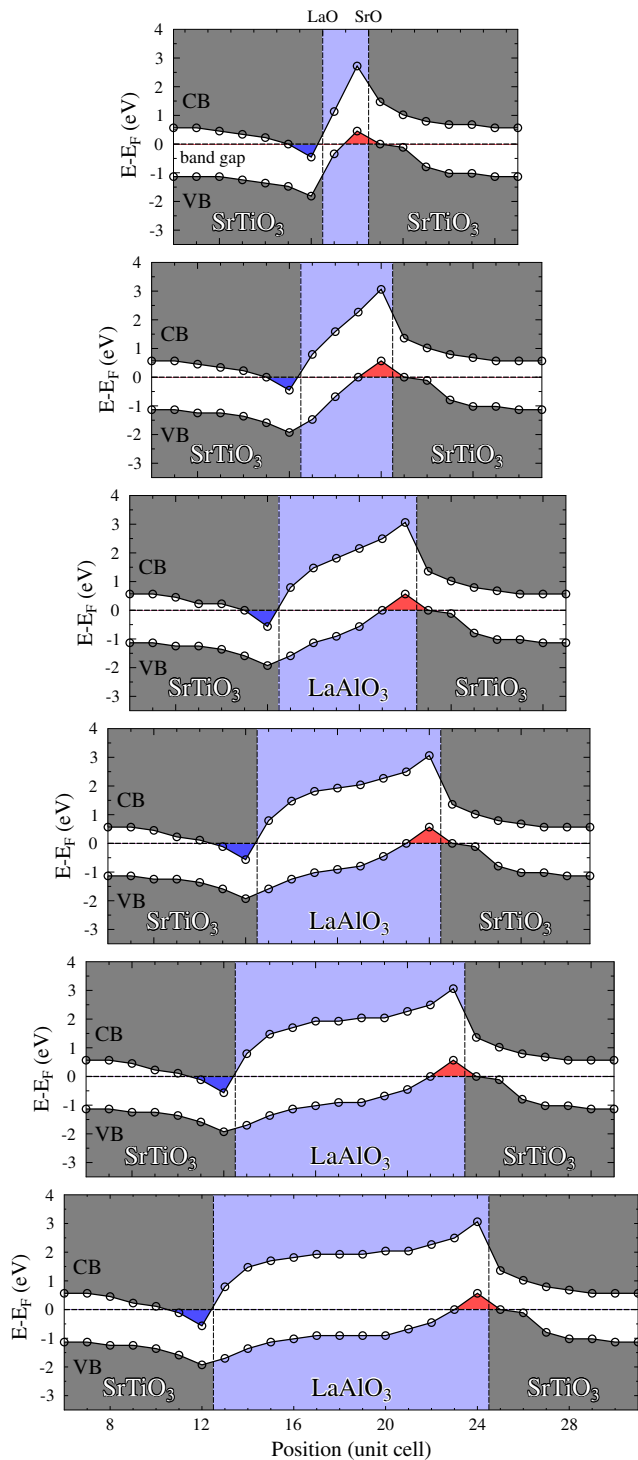
Figure 1. Calculated CB and VB profiles for the [001] direction of LAO/STO(001) superlattices with LAO thicknesses from 2 (top) to 12 u.c. (bottom). The dark blue region indicates the 2DEG and red the 2DHG. (Motivated by Ref. [44].)

(**Figure 1**). As LAO is polar and asymmetric, the 2DEGs (red) and 2DHGs (blue) appear together regardless of the LAO thickness.

Apart from the polar discontinuity, the potential step between STO and LAO forms the band bending: the thinner the LAO, the larger the bending. The band-edge profile calculated for the 2-u.c.-thick LAO resembles that of ferroelectrics (the 2DEG between STO and a robust ferroelectric, such as BaTiO$_3$ or PbTiO$_3$, has been recently anticipated from first principles[47,48]).

In LAO/STO(001), the band bending seems strong enough to develop simultaneously 2DEG and 2DHG even in the case of ultrathin LAO, that is, below the critical thickness of 4 u.c. In other words, the chosen geometry does not reproduce this critical thickness. However, for ultrathin LAO its surface and intrinsic defects would lead to substantial structural changes, which were taken into account.

The geometry of ideal 12 u.c./12 u.c. LAO/STO(001) is shown in **Figure 2**a. At the n-type (p-type) interface, each interfacial Ti (Al) atom has six nearest O atoms, four next-nearest Sr,
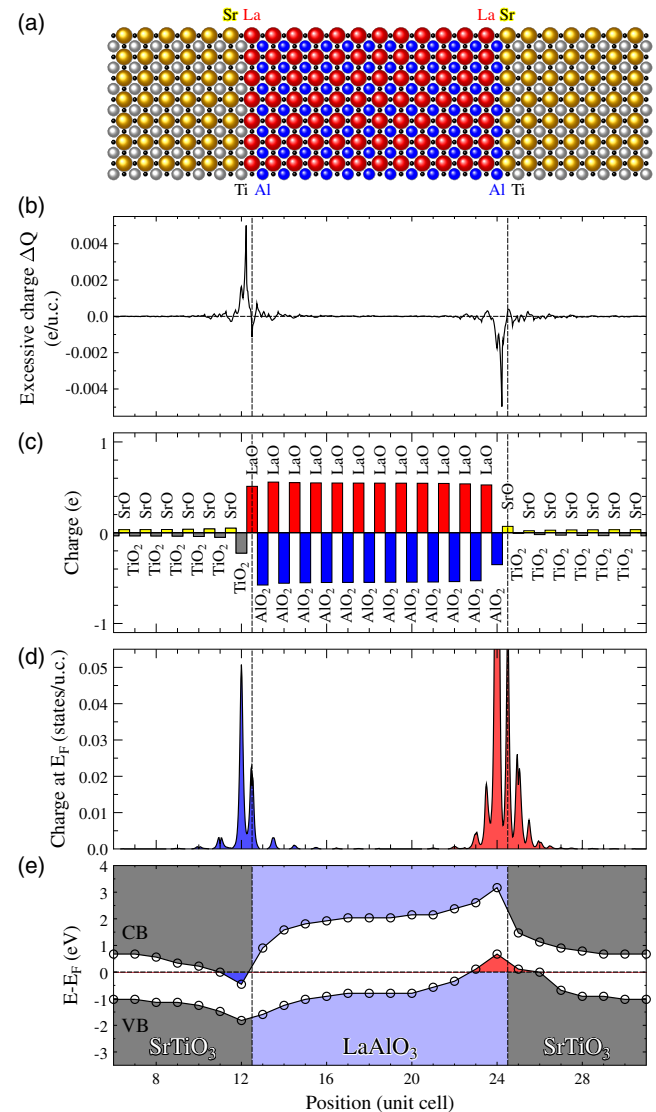

Figure 2. a) Geometry, b) excessive interface charges, c) layer-resolved charges, d) free charges at E_F, and e) the CB/VB profile along the [001] direction of LAO/STO(001), constructed as a 12 u.c./12 u.c. supercell. In (a) the La, Al, Sr, and Ti positions are shown by red, blue, golden, and grey balls, respectively, whereas the black dots depict oxygen sites. (Motivated by Maznichenko et al.[44])

and four next-nearest La atoms. The polar discontinuity at both terminations of LAO should be screened; as a result, the 2DEG and the 2DHG appear there (Figure 2e).

To illustrate this screening we compute the charges within Wigner–Seitz cells around each ion and sum these over each [001] layer. The LaO and AlO$_2$ layers are charged oppositely by $\approx +1/2$ and $\approx -1/2$ electron charge, respectively, whereas the SrO and TiO$_2$ layers of STO are almost neutral except at the interfaces. At the n interface, the TiO$_2$ layer becomes negatively polarized (Figure 2c), with the charge less than half of that of its neighboring LaO partner. This may reduce the oxidation state of interfacial Ti from typical 4+ in bulk STO to 3.5+.

The site-projected and layer-resolved densities of states (DOSs) $n(E)$ are shown in **Figure 3**, with the two upper panels

displaying the differences in the DOSs between interfacial and another Ti placed in the sixth u.c. of STO. The DOS of the latter Ti is similar to that of Ti in bulk STO. The $n(E)$ of the interfacial Ti at energies below the Fermi level (E_F) is dominated by the 3d$_{xy}$ states (Figure 3c) and indicates metallicity, thereby manifesting the 2DEG.

Regarding the p interface, interfacial SrO is charged positively but insignificantly (Figure 2c), whereas the nearest AlO$_2$ layer looses its negative charge by about 1/3. Nevertheless, the oxidation state of interfacial Al, 3+, remains unchanged. These results confirm previously reported ab initio calculations.[29,49,50]

To discuss the 2DHG at the p interface of LAO/STO(001), we depict in **Figure 4** the total and three partial p DOS calculated for O in the AlO$_2$ interfacial layer. The O p states form the topmost valence band of the system. Therefore, only the O p$_x$ states of this interfacial O spill above E_F and, therefore, develop the 2DHG effect. The second interfacial O atom (not shown here) in the AlO$_2$ layer contributes to 2DHG with p$_y$ states, where the z-axis is oriented along [001].

There are a few intrinsic factors that affect quantitatively the 2DEG. As the LAO lattice parameter of 3.79Å is less than that of the STO(001), we expect tetragonal compression of about 2% in the LAO layers. For the ideal and cubic LAO/STO(001) superlattice, its 2DEG (2DHG) carrier density g_e (g_h) at the Fermi level is 0.8×10^{13}cm^{-2} (3.4×10^{13}cm^{-2}), whereas tetragonally compressed LAO enhances this number up to 1.4×10^{13}cm^{-2} (4.3×10^{13}cm^{-2}). Further structural optimization near the interfaces may enhance the 2DEG magnitude, similarly to that of tetragonally compressed LAO.[38]
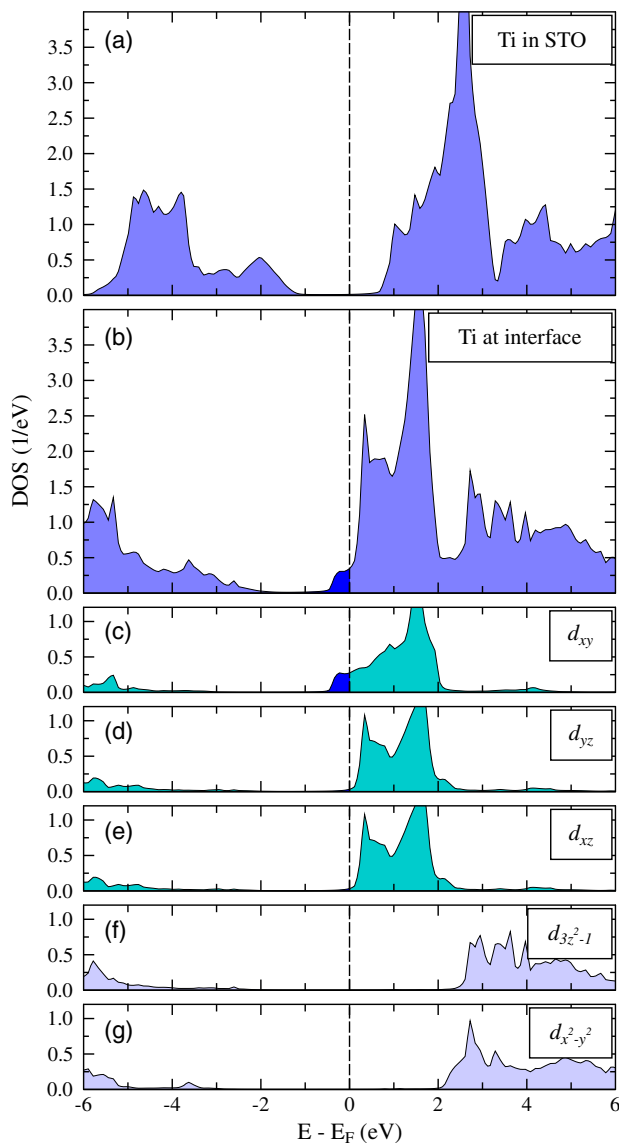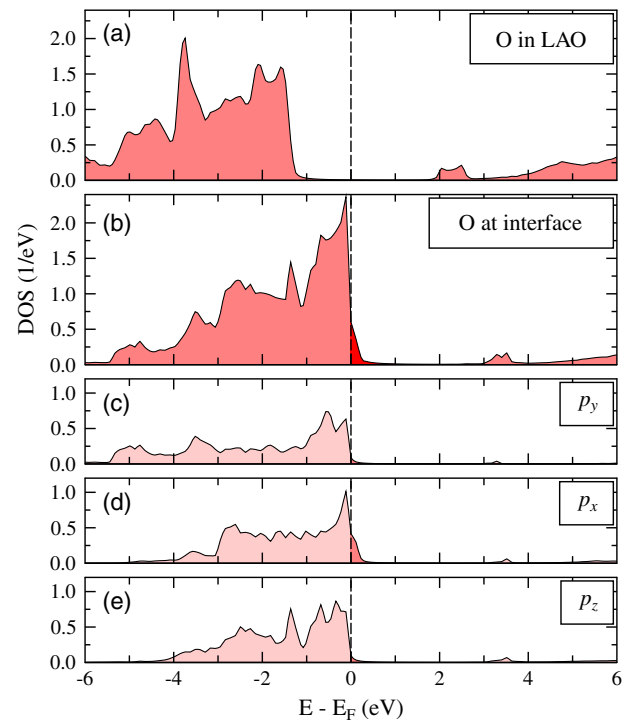

Figure 3. DOSs projected on selected Ti sites in LAO/STO(001). a,b) The total DOSs of the 'bulk-like' and interfacial Ti, respectively. c–g) The partial 3d contributions to the DOS of interfacial Ti. (Motivated by Maznichenko et al.[44])

Figure 4. a,b) Oxygen DOSs in LAO/STO(001) calculated for the bulk-like LAO site and interfacial O site of the AlO$_2$ layer, respectively. c–e) The three p-orbital contributions of interfacial O. (Motivated by Maznichenko et al.[44])

2.1.2. SrTiO₃/KTaO₃(001)

KTaO₃ (KTO) is a wide-gap polar perovskite, the (001) layers of which represent alternately charged $[KO]^-$ and $[TaO_2]^+$ planes. Epitaxial growth of KTO is problematic because of very reactive potassium atoms. However, the KTO(001) surface can be used to grow STO overlayers. The TaO_2/SrO-terminated STO/KTO interface, therefore, should exhibit a 2DEG, whereas the TiO_2/KO termination is suitable for a 2DHG. So far, the polar nature of KTO(001) has been realized in O-deficient top layers, which is achieved by Al capping layers.[51]

In this work, we anticipate from first principles the 2DEG/2DHG formation at ideal interfaces of STO/KTO(001). The 12 u.c./12 u.c. superlattice, with the STO lattice parameter, is used for this (**Figure 5**). As panel(c) shows, the band bending at the STO/KTO(001) interfaces is similar to that of LAO/STO(001), although the 2DEG and 2DHG seems to be differently distributed between the interfacial layers. In particular, the 2DEG of STO/KTO(001) is accommodated about equally between the polar and STO sides, whereas the 2DEG of LAO/STO(001) is accommodated almost exclusively in a few layers of STO. In this context, it is worthwhile to perform simulations of STO/KTO(001) for geometry-optimized instead of uniformly compressed one KTO.

2.1.3. LaFeO₃/SrTiO₃(001)

A conducting 2DEG at the interface between the STO(001) surface and epitaxial LaFeO₃ (LFO) has been observed recently.[12] An LFO overlayer thicker than 3 u.c. is needed to produce the 2DEG, which itself is sensitive to cation intermixing and oxygen
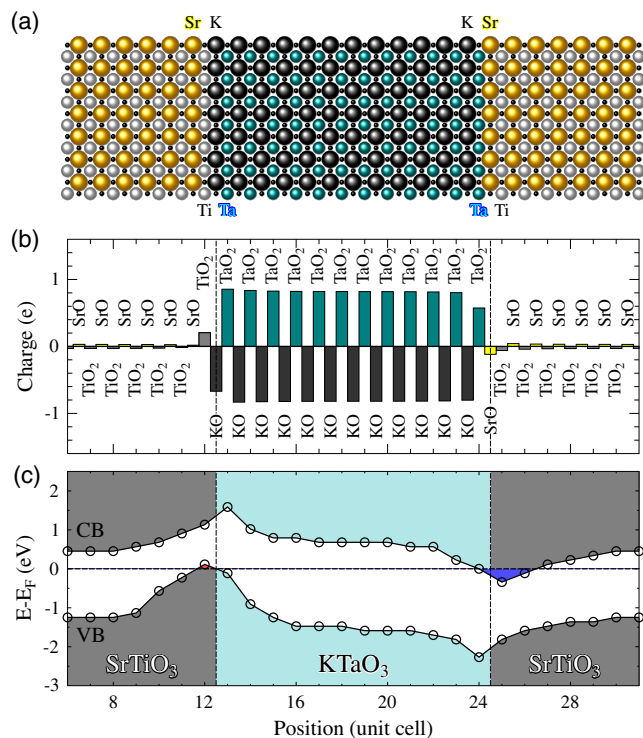
nonstoichiometry. Most importantly, ionic liquid gating allows for robust control of the 2DEG formation, thereby forming a nonvolatile switch. These experimental findings have been supported by ab initio calculations.

In **Figure 6**, the [001] band-edge profile of LFO/STO(001) calculated for a 12 u.c./12 u.c. superlattice is shown. The 6 u.c. thick LFO enables the 2DEG/2DHG formation at the TiO_2/LaO and FeO_2/SrO-terminated interfaces. We conclude that the band bending within LFO as well as the 2D carrier densities are compatible to those of the 12 u.c. thick LAO in LAO/STO shown in Figure 1.

Although the 2DHG appears in ab initio calculations for superlattices constructed from polar and nonpolar perovskites, the corresponding measurements and their interpretation appear questionable. This requires a heterostructure prepared practically without defects. Oxygen vacancies at the p interface may suppress the 2DHG. Until now, there is only one ambitious report on a 2DHG detected in LAO/STO(001).[52] The coexistence of 2DEG and 2DHG in ultrathin LAO layers below its critical thickness has been discussed recently.[53] The main target is robustly controlled 2DEG. For that reason, the research usually grows polar perovskite overlayers to form the 2DEG beneath, removing therefore the p interface.

2.2. Polar/Polar Interface

2.2.1. LAO/STO(110) and LAO/STO(111)

As (110) and (111) layers of STO are charged, the corresponding LAO/STO interfaces are polar from both sides. We now discuss ideal LAO/STO(110) and LAO/STO(111) superlattices.
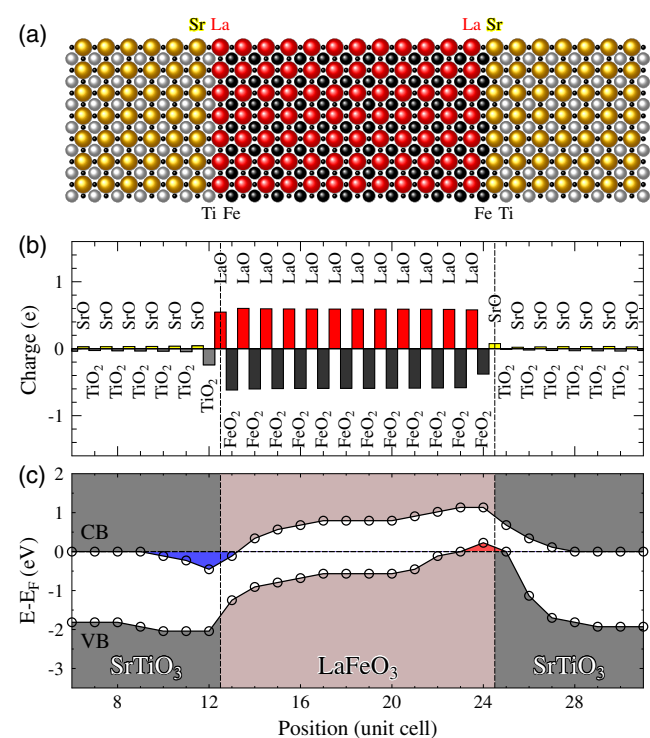

Figure 5. a) Geometry, b) layer-resolved polarity, and c) band bending of a STO/KTaO₃(001) superlattice.

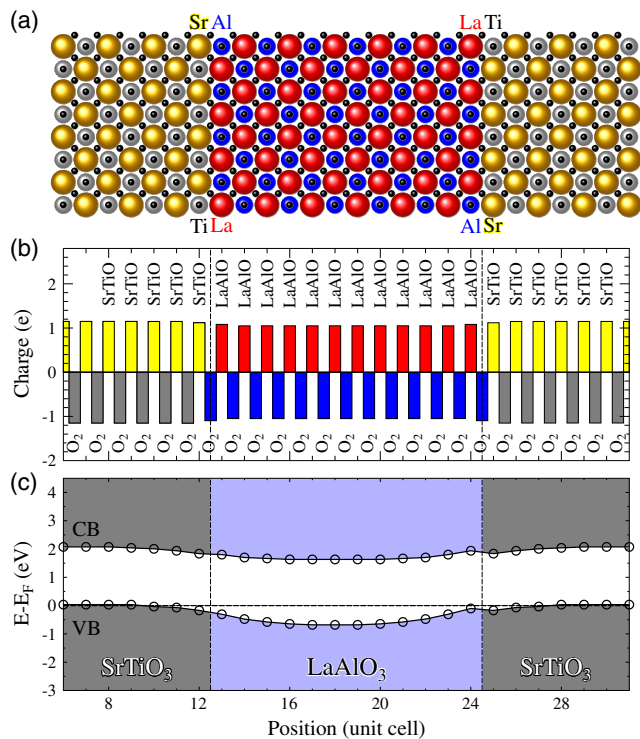**Figure 6.** a) Geometry, b) layer-resolved polarity, and c) band bending of a LFO/STO(001) superlattice.

Figure 7. a) Geometry, b) layer-resolved polarity, and c) band bending of LAO/STO(110). (Motivated by Maznichenko et al.[44])

Figure 8. Same as Figure 7, but for LAO/STO(111). (Motivated by Maznichenko et al.[44])

Charges and the band-edge profiles are shown in **Figure 7** and **8**, respectively. In the case of LAO/STO(110), each interfacial Ti has six next-nearest Sr and two La atoms. The layer-resolved charges in **Figure 8**b change smoothly at the interfaces, that is, without polar discontinuity; therefore, neither 2DEG nor a 2DHG is formed since the conduction/valence bands are bent marginally. Taking into account the buckling at the LAO/STO(110) interface, however, a 2DEG with strongly anisotropic conductivity was found.[54] Ab initio calculations performed to explain these findings suggest[54] that the TiO-terminated buckled (110) surface of STO is energetically more favorable than a polar stoichiometric one. If this reasoning is valid, then a 2DEG can be developed at the buckled (110) interface because of occasional (001) islands and their stronger polar discontinuity.

Our results for LAO/STO(111) are collected in Figure 8. The system obeys a threefold rotational symmetry. Interestingly, the STO(111) layers are more polar than the LAO layers. The polar discontinuity is less pronounced than in LAO/STO(001). The band bending, shown in Figure 8c, is slightly enhanced with respect to that of LAO/STO(110), but is significantly weaker as compared to LAO/STO(001). In perfect LAO/STO(111), thus, the topmost valence band touches E_F, but the carrier concentration of the 2DHG is marginal; a 2DEG is not formed.

Experiments often report that (110) and (111) interfaces of LAO/STO can be made conductive, with carrier density and electronic mobility similar to those of the (001) interface.[55,56] More precisely, a transition to metallicity was observed for critical thicknesses of 7 MLs and 9 MLs for (110) and (111) interfaces, respectively. The increased number of layers may be explained by the reduced interlayer distances compared to the (001) case,
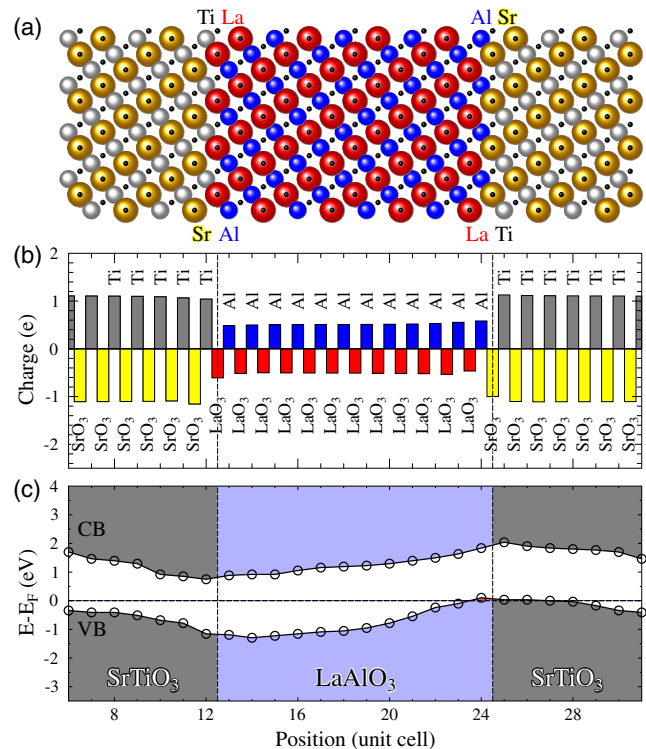
which conforms with all critical thicknesses being close to each other: 16 Å for (001), 19 Å for (110), and 20 Å for (111).

2.2.2. KTO/LAO(001)

Both perovskites of KTO/LAO(001) are polar and its n (p) TaO$_2$/ LaO (AlO$_2$/KO) interface has excessive electrons (holes) from both sides (**Figure 9**). As a result, the 2DEG and the 2DHG seem more expectable. However, the corresponding interfacial charge densities are less than expected from broken consequence of polar layers at the interface from both sides LAO and KTO. Moreover, the epitaxial interfaces of KTO/LAO(001) look like hypothetical ones. The measured KTO lattice parameter of 3.99 Å is significantly larger than that of LAO 3.79 Å. Therefore, the lattice mismatch of 5% may prevent defectless growth of KTO/LAO(001). In our calculation, we used the intermediate lattice constant of STO.

In summary, we present earlier the two options of the polar/ polar perovskite interfaces, studied from first principles within the superlattice model. This scenario, however, does not improve the 2DEG formation. For the latter, the polar overlayers grown on a STO(001) substrate represent the most likely scenario.

3. Defective LAO/STO(001) Superlattices

3.1. Coherent Cation Intermixing

Typical imperfections that appear at (001) interfaces of epitaxially grown perovskites are steps at which the cations of one
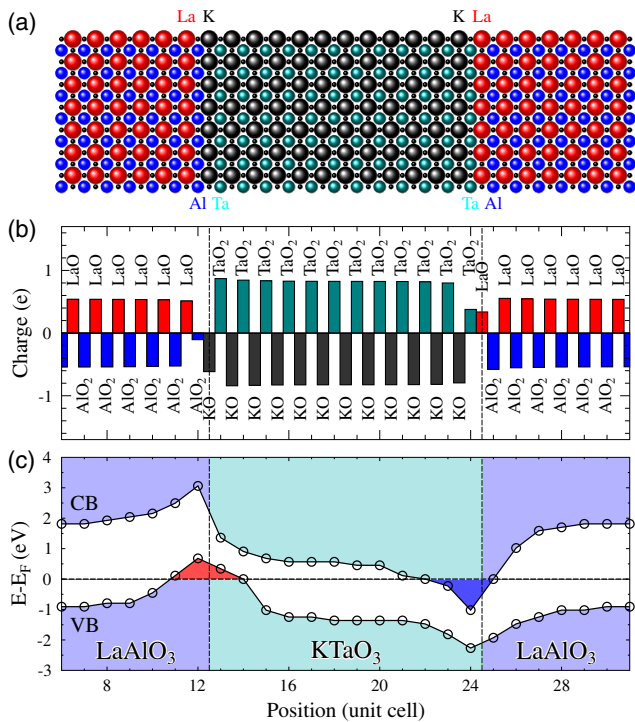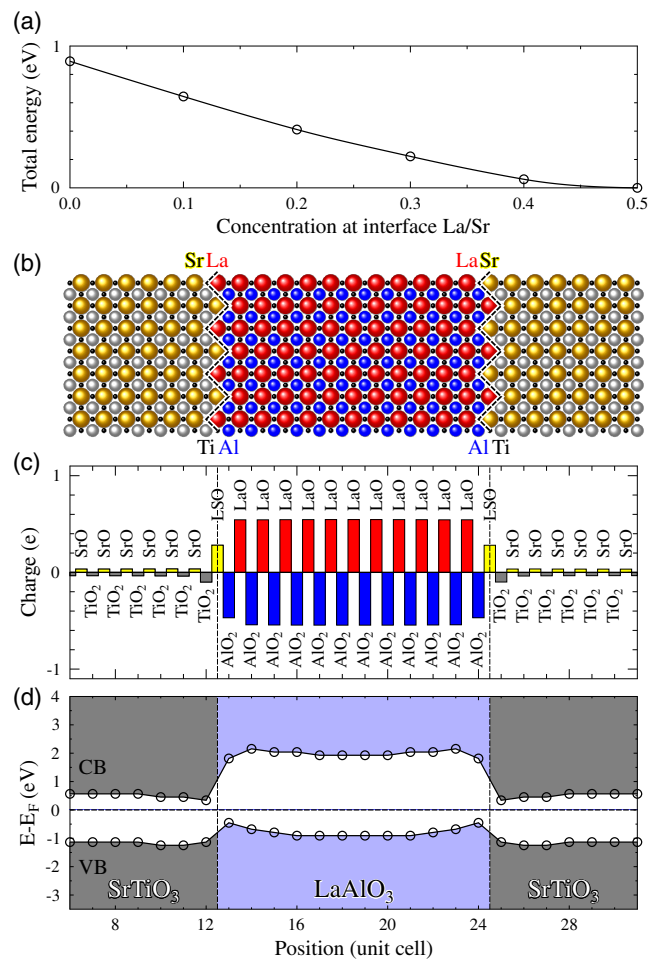
Figure 9. Same as Figure 7, but for KTO/LAO(001).

Figure 10. Properties of LAO/STO(001). a) Total energy versus substitutional disorder x in the interfacial $La_{1-x}Sr_xO$ and $Sr_{1-x}La_xO$ layers. b) Geometry, c) polar discontinuity, and d) band profile calculated for $x = 0.5$. (Motivated by Maznichenko et al.[44])

perovskite substitute the corresponding cations of the other. The step heights range usually between one u.c. and two u.c., depending on the growth conditions. Recall that producing a sharp interface is hardly possible and that cation intermixing across the LAO/STO interface changes the charge distribution and affects the 2DEG/2DHG.

At the n interface of LAO/STO(001), candidates for mixing are La and Sr. The Sr species appears largely at the La sublattice, for instance, in $La(Sr)MnO_3$. Here, we model, within the GF method and the CPA, the La/Sr intermixing that goes on simultaneously across the n and p interfaces by varying the Sr (La) concentration in interfacial LaO (SrO) between 0 and 50 at%. As the amount of each species is conserved in the superlattice, total energies can be compared, the latter calculated for each chosen Sr content x in the interfacial $La_{1-x}Sr_xO$ layer. The total energy decreases with increasing x (**Figure 10**a) and, therefore, the 1:1 La/Sr intermixing is energetically favored by $0.9\,eV\,u.c.^{-1}$ surface area of LAO/STO(001). Most importantly, the 2DEG disappears completely as $x \to 0.5$, as shown in Figure 10d. This is related to the LAO critical thickness of about 1.6nm. The excessive and opposite charges of 2DEG/2DHG act like a planar capacitor for the LAO thicknesses above critical.

To analyze the effect of coherently mixed cations on the 2DEG, we show in **Figure 11** the DOS of interfacial Ti versus x. The Ti DOS of the perfect interface ($x = 0$) is shown in the top panel, whereas its lower panel shows how the DOS changes when the La/Sr mixing varies between 0 and 1. The Ti DOS and the total DOS at the Fermi level $n(E_F)$ completely vanish for $x > 0.4$. Using the $n(E_F)$ values, we calculated the 2DEG density $g_e(x)$, which is very sensitive to the DOS details near E_F (**Figure 12**). With increasing x, $g_e(x)$ increases insignificantly at around

$x = 0.1$ due to the shallow Ti DOS at $-0.3\,eV$ (Figure 3). At larger x, $g_e(x)$ decreases monotonically to marginal values (e.g., $x > 0.4$). For the n-type interface we modeled the B-cation step, replacing interfacial Ti by Al in the $Ti_{1-x}Al_xO_2$ layer. These results are shown in Figure 12 as well.

The corresponding electron density $g_e(x)$, calculated at E_F as a function of the Al content, decreases with increasing x similarly to the case of La/Sr. Thus, for the n interface of LAO/STO(001) we anticipate that its 2DEG can be completely suppressed by coherently mixed cations for $x > 0.4$. It should be noted that such a scenario assumes a superlattice and, therefore, requires cation mixing at the p interface as well. In practice, the 2DEG is observed below LAO overlayers, that is, in systems with electronically reconstructed $AlO_2(001)$ surfaces.

3.2. Interfacial Cation Substitutes

Now we address cation substitutes near the LAO/STO interfaces,[3,57] which differ from the coherent intermixing of cations discussed previously. The effect of annealing may cause
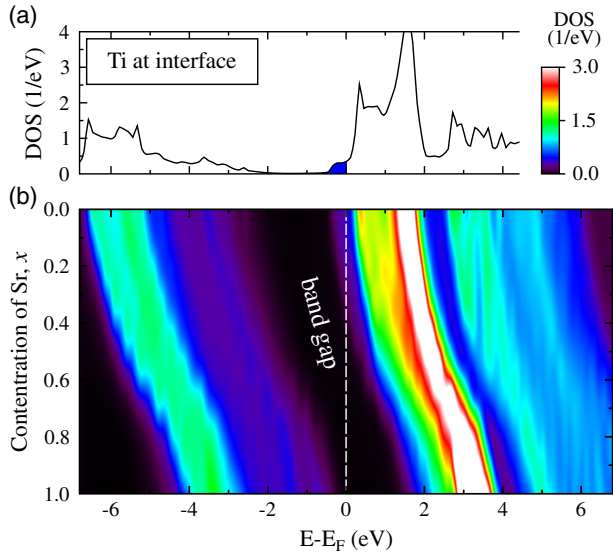
Figure 11. DOS of interfacial Ti at the $La_{1-x}Sr_xO/TiO_2$-terminated interface of LAO/STO(001) for a) $x = 0$ and b) as color scale, versus the Sr content x. (Motivated by Maznichenko et al.[44])
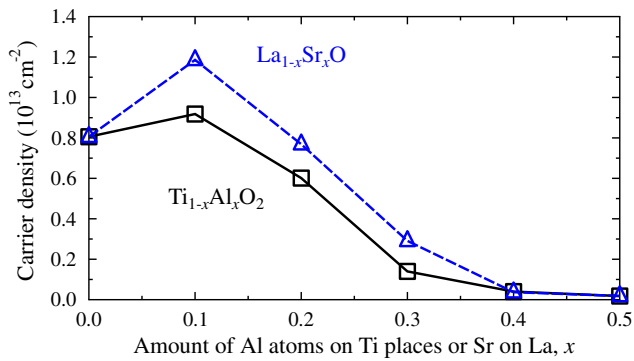

Figure 12. 2DEG density at the Fermi level of the n-type LAO/STO(001) interface versus the Sr (Al) content x in the interfacial $La_{1-x}Sr_xO$ ($Ti_{1-x}Al_xO_2$) layer represented by a red (black) line. (Motivated by Maznichenko et al.[44])

diffusion of cations off the interface. Such changes in the cation composition at the n interface may be independent from that at the p interface. We consider the scenario when the interface remains atomically sharp while atom swapping takes place within the two u.c. The CPA was used within the supercell model to mimic incoherent swapping of cations near each interface of LAO/STO; interstitial cation positions were excluded.

Regarding the 2DEG (**Figure 13**a), g_e gradually increases with increasing x. However, the enhancement is more pronounced for the B-cation intermixing $Ti \leftrightarrow Al$. This is not surprising as the 2DEG is formed by the Ti d states (Figure 3). As concerns the 2DHG at the p interface (**Figure 14**a), its density g_h also increases with x. The B-cation intermixing enhances g_h more efficiently than the A-cation intermixing, which is explained as follows: holes emerge mostly in the AlO_2 layer near the p interface and, thus, the intermixing $Ti \leftrightarrow Al$ is more efficient for g_h. Most importantly, there is a key difference to the 2DEG at the
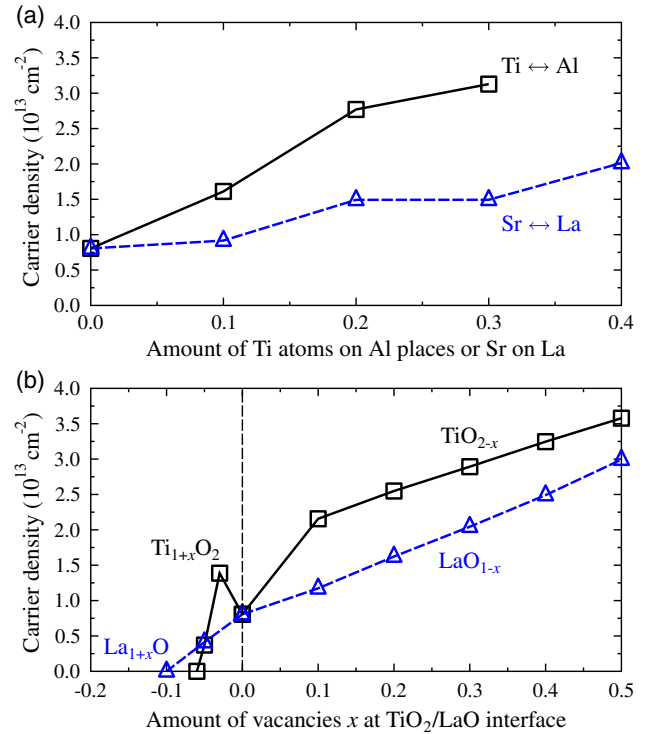

Figure 13. 2DEG density at the Fermi energy $g_e(E_F)$ formed at the n interface of LAO/STO. a) g_e is shown by a red (black) line versus the A (B)-cation substitutes x. b) g_e is shown versus the oxygen ($x > 0$) or cation ($x < 0$) vacancy rate in the LaO (blue) and TiO_2 layers (black line). (Motivated by Maznichenko et al.[44])
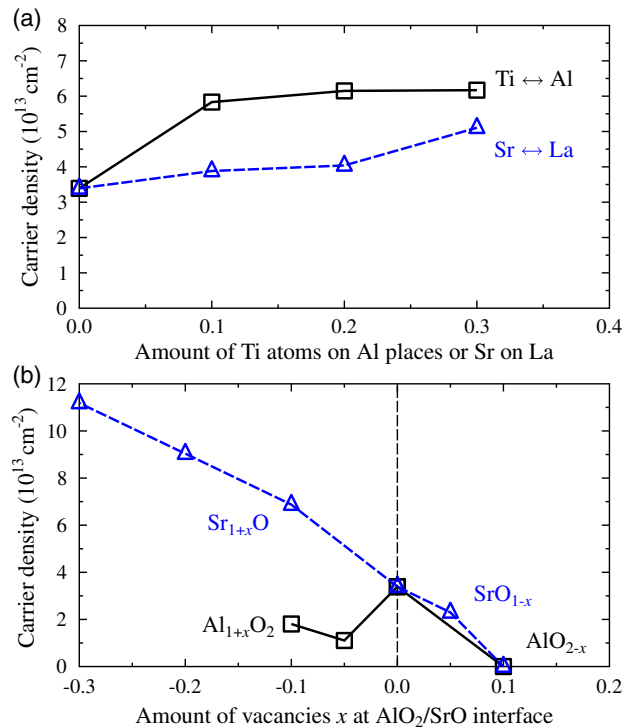

Figure 14. Same as Figure 13, but for the 2DHG density at the Fermi level of a p interface of LAO/STO(001). (Motivated by Maznichenko et al.[44])

cation substitute containing LAO/STO(001) between the coherent and incoherent (single-interface) intermixing that is evident by comparing Figure 12 with Figure 13a. For the latter case, g_e increases remarkably with x, whereas the two-interface coherent intermixing suggests the opposite trend and suppresses the 2DEG completely at $x > 0.4$.

3.3. Oxygen and Cation Vacancies

3.3.1. 2D Response to the Doping at the Same Interface

Oxygen vacancies are the common defects in epitaxially grown perovskites. We model oxygen vacancies at each interfacial layer of LAO/STO(001). As one may expect, O vacancies, that is, n doping, enhance the 2DEG effect at the n interface, which is shown for $x > 0$ in Figure 13b for the LaO_{1-x} and TiO_{2-x} interfacial layers. The cation vacancy, that is, p doping at the n interface, was simulated as well. The corresponding g_e are shown also in Figure 13b for negative x in the interfacial compositions $La_{1+x}O$ and $Ti_{1+x}O_2$. Obviously, p doping reduces g_e, so a 2DEG may be removed completely by the presence of Ti (La) vacancies of 5 at% (10 at%) at the n interface.

The 2DHG effect at the p interface may be enhanced by p doping, shown in Figure 14b for $x < 0$. By contrast, O vacancies ($x > 0$) in the interfacial layers SrO_{1-x} and AlO_{2-x} suppress the 2DHG effect (Figure 14b). These findings agree with experimental reports that the concentration of oxygen vacancies is 0.32 ± 0.06, whereas a 2DHG could not be detected.[3]

3.3.2. 2D response to the Doped Remote Interface

So far we focused on the 2D gas variations occurring due to doping at the same interface. However, 2DEGs and 2DHGs interact through the insulating layers. When the charge balance changes at one interface (for instance, a p interface) this modifies the Fermi level in the system and, therefore, the charge density may vary at the other interface (n interface).

For the LAO/STO(001) superlattice, this effect is visualized in **Figure 15**. For LAO/STO with 10% O vacancies in the interfacial $AlO_{1.9}$ layer, O vacancies should suppress the 2DHG that appears in the defectless case (Figure 2e). We anticipate that for O vacancy compositions >10% the 2DHG disappears completely, whereas 2DEG enhances slightly. The top of the valence band that appears below the Fermi level occurs at the $AlO_{2-\delta}$ interfacial layer with $\delta = 0.1$.
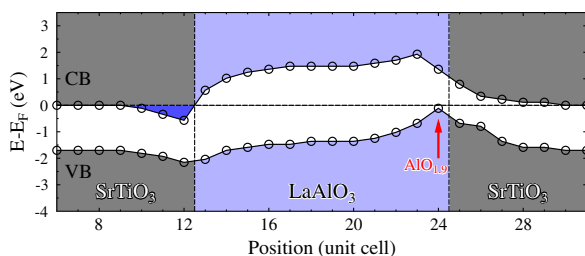

Figure 15. CB/VB profile along [001] of the LAO/STO(001) superlattice calculated for a 10% O-deficient p interface.
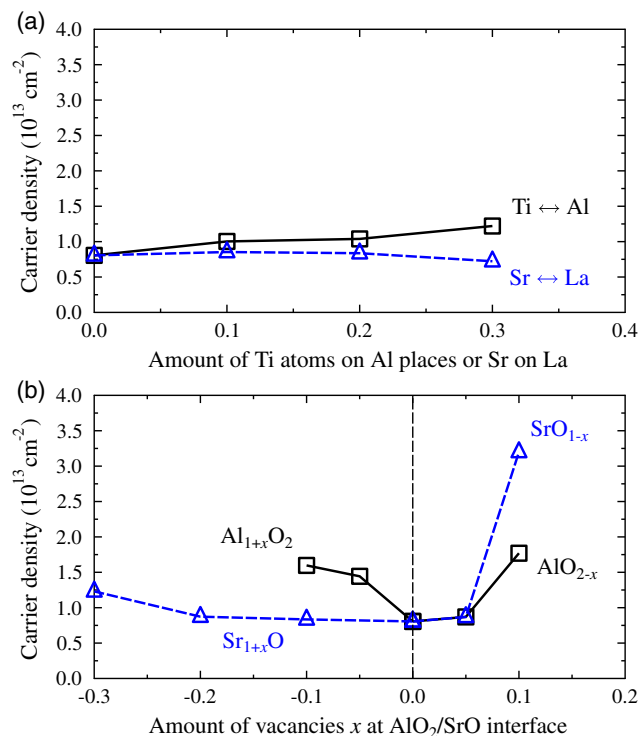

Figure 16. 2DEG density at the Fermi energy $g_e(E_F)$ at the n interface of LAO/STO. a) g_e is shown by the red (black) line as a function of the A (B)-cation substitutes, x. b) g_e is plotted against the oxygen ($x > 0$) or cation ($x < 0$) vacancies in the SrO and AlO_2 layers by blue and black lines, respectively.

More detailed results of the simulated effect of distant doping are collected in **Figure 16** and **17**. The needed 2DEG density can be tuned remotely via the p interface. Although our calculations rely on the ideal structure of the defective interfaces of LAO/STO(001), our findings open a path for prospective applications for tuning 2DEGs.

3.4. LAO/STO(001) Overlayers

3.4.1. Effect of an Ideal LAO Surface

The conduction band (CB)/valence band (VB) profiles for 8 u.c. thick LAO(001) on 12 u.c. thick STO are shown in **Figure 18**. We assume that a cubic crystal structure with the LAO surface is AlO_2-terminated and the TiO_2/LaO interface is perfect. The bandgap shown in Figure 18 is calculated from the DOS within TiO_2 and AlO_2 layers only. It clearly shows that a 2DEG emerges at the TiO_2/LaO interface and a weakly p-doped LAO surface.

The 2DEG density integrated over a few interfacial layers along [001] is 3.2×10^{13} cm^2, that is, 4 times larger than the 2DEG density of the ideal superlattice. **Figure 19** shows the layer-resolved contributions calculated near the n-type interface for a slab with an ideal LAO surface and for a heterostructure with chemically perfect interfaces. The 2DEG becomes more pronounced for the surface. For the heterostructure, the LAO thickness is 8 u.c., whereas its 2DEG density differs insignificantly from that of the 12 u.c.-thick.
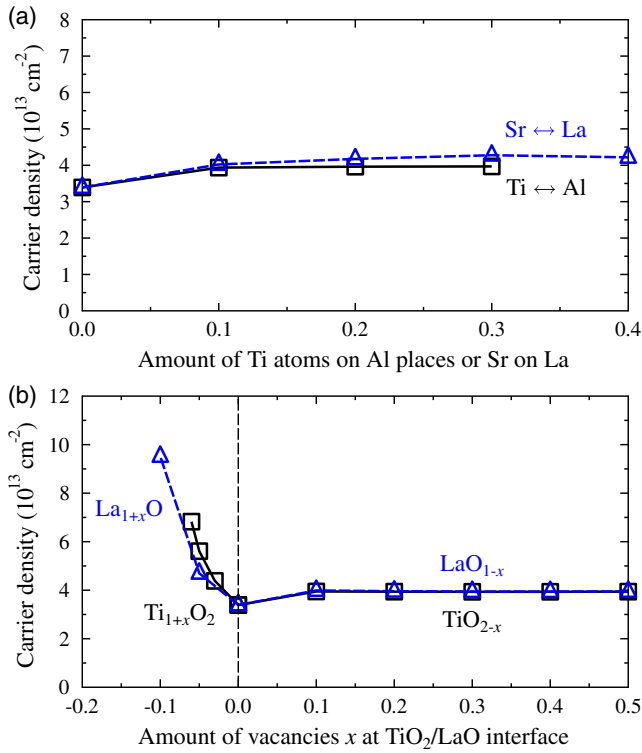
Figure 17. 2DHG density at the Fermi level of the AlO$_2$/SrO-terminated interface of LAO/STO(001). a) g_h is shown by the red (black) line as a function of the A (B)-cation substitutes, x. b) g_h is plotted against the oxygen ($x > 0$) or cation ($x < 0$) vacancies in the LaO and TiO$_2$ layers by blue and black lines, respectively.
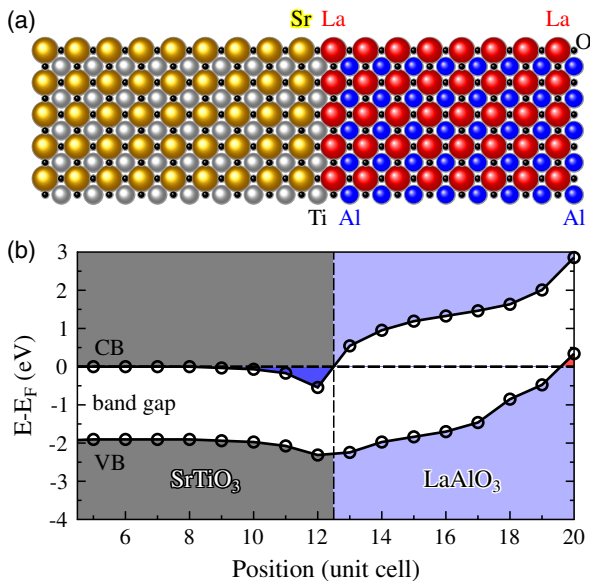

Figure 18. a) Geometry and b) the CB/VB profiles along [001] of 8 u.c. thick LAO(001) grown on 12 u.c. thick STO. a) Red balls depict La atoms, blue Al atoms, golden Sr atoms, and gray Ti atoms. Black dots show oxygen atoms. (Motivated by Maznichenko et al.[45])
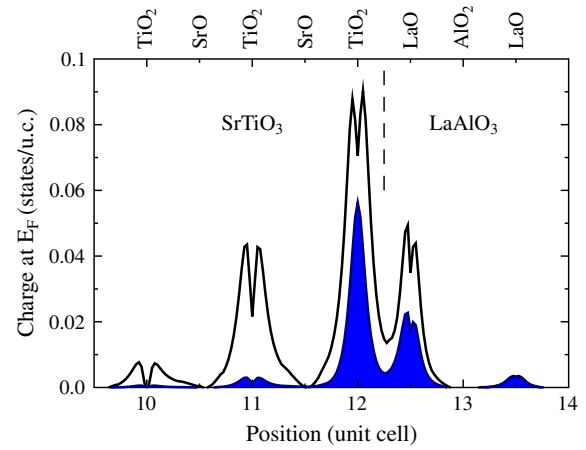
Figure 19. Layer-resolved contributions to the 2DEG for a perfect LAO/STO superlattice (filled blue) and a chemically perfect LAO/STO(001) surface (black solid line). A LAO thickness of 8 u.c. was used for both cases. Atomic layers are labeled and numerated along [001]. (Motivated by Maznichenko et al.[45])

The topmost AlO$_2$ layer of LAO(001) is corrugated: O positions are above Al positions.[58,59] We computed the 2DEG density for a system with relaxed atomic positions in the topmost layer (**Figure 20**). The result indicates that the 2DEG density increases by 0.2×10^{13} cm^2 compared to that of an unrelaxed surface. In addition, we varied the O displacements from the surface AlO$_2$ layer between -0.08 and 0.12 Å: the 2DEG density gradually increases when the O–Al separation increases within the topmost layer.

3.5. Effect of Oxygen Doping at the LAO Surface

We simulated both O vacancies and excessive oxygen compositions at the surface, which mimics to some extent the effect of liquid gating (**Figure 21**). In the case of an oxygen-deficient surface, AlO$_{2-\delta}$, with increasing $0 < \delta < 0.1$ the 2DEG density increases up to 3.6×10^{13} cm^2. For $0.1 < \delta < 0.2$, the calculated density of 2DEG remains robustly larger than 3.5×10^{13} cm^2. For the O-rich LAO surface, AlO$_{2+\delta}$, the 2DEG density increases

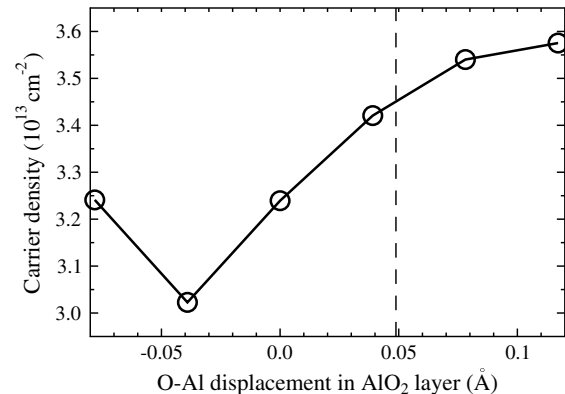**Figure 20.** 2DEG density of LAO/STO(001) as a function of the O–Al displacement within the surface AlO$_2$ layer. The vertical dashed line marks the O positions after relaxation. (Motivated by Maznichenko et al.[45])
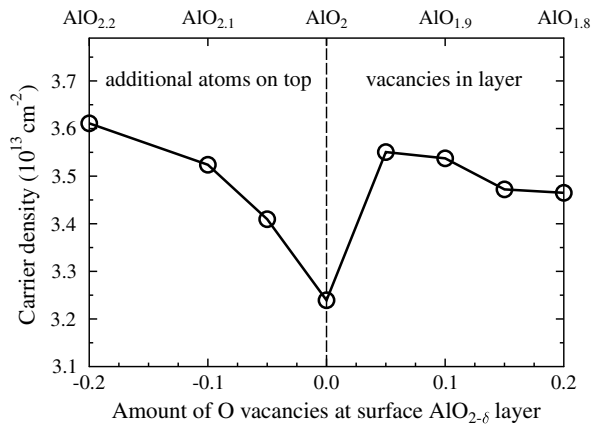
Figure 21. 2DEG density at an n-type LAO/STO(001) interface versus oxidation degree of the surface $AlO_{2-\delta}$ layer. (Motivated by Maznichenko et al.[45])

Figure 22. Bloch spectral function, projected on the interfacial TiO_2 (AlO_2) layer of an n (a p) interface of LAO/STO(001) plotted in the upper (lower) panels along the high-symmetry directions of the 2D Brillouin zone.

gradually with δ. This effect of a doped surface is similar to that shown in Figure 16 for a LAO/STO superlattice.

The enhanced 2DEG for the surface composition $AlO_{2+\delta}$ is understood in terms of dipole interactions between the p-charged surface and the n-charged interface. With an increasing number of holes at the surface, the band bending results in a surplus of interfacial electrons to keep the charge balance. The case of $AlO_{2+\delta}$ may seem artificial as this composition is energetically not favorable. A relaxed oxide surface always tends toward charge neutrality. In this context, the O-deficient surface composition $AlO_{2-\delta}$ represents a more reliable scenario.

4. Transport-Related Details of 2DEG

4.1. Ideal Superlattice LAO/STO(001)

To provide better insight into the electronic states that form the 2DEG and which determine the transport properties, we choose an LAO/STO(001) interface. Starting from the dually terminated superlattice, we address the Bloch spectral function projected on the interfacial layers of LAO/STO(001) along high-symmetry directions of the 2D Brillouin zone (**Figure 22**). At the n-type interface (upper panels), the Ti d band crosses E_F near Γ. As for the p interface of LAO/STO(001), the O p-states of the valence band "spill into" the bandgap around M.

The conduction bands that cross E_F near Γ exhibit isotropic dispersion; refer to the spherical Fermi contour in the top row of **Figure 23**. The Ti d-states of the TiO_2 layer contribute mostly to the Fermi surface cross section. The corresponding $E(k)$ is almost parabolic (Figure 22), with an estimated effective electron mass of $0.38m_e$. The effective masses reported so far range between $0.41\,m_e$[38,60] and $0.52\,m_e$, or exhibit even larger values.[61]

Theory suggests that a 2DHG should appear at the AlO_2/ SrO-terminated interface of a LAO/STO(001) superlattice. Nevertheless, the experimental observation of a 2DHG is still a subject of debate. Until now, there is—to the best of our knowledge—a single report on a 2DHG detected in LAO/STO(001).[52]
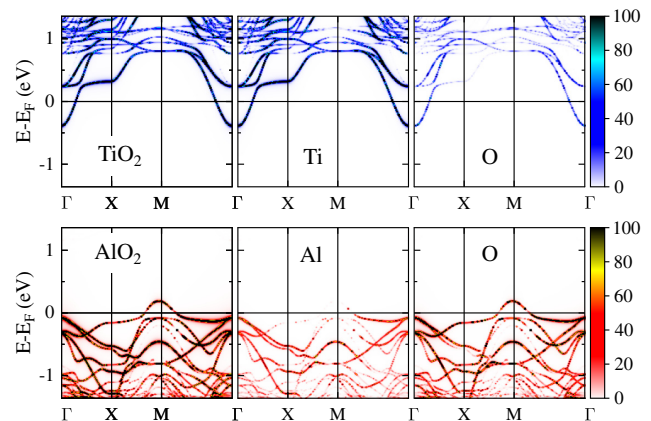
Regarding the electronic states near the p interface, the corresponding Fermi contours have fourfold symmetry, as is evident from the bottom row of Figure 23. The 2DHG's effective mass is strongly anisotropic, ranging between $0.79\,m_e$ for the $M-X$ and $1.06\,m_e$ for the $\Gamma-M$ direction, respectively. Thus, the effective mass is two times larger than that of 2DEG. This finding allows us to estimate the 2DHG's mobility and to understand why a 2DHG was not observed until now.

4.2. LAO Overlayer on STO(001)

Key features of electronic states of the n interface LAO/STO(001) formed by the LAO overlayer are shown in **Figure 24**. Using a GF technique for a supercell with vacuum, we calculated the Bloch spectral function projected onto the interfacial TiO_2 layer and its Ti and O sites. Figure 24 shows how the Ti d conduction band crosses E_F around Γ, whereas the O contribution is the result of hybridization with the Ti d orbitals.

A superlattice without vacuum exhibits an isotropic conduction Ti d band that forms a 2DEG in LAO/STO; refer to the spherical Fermi contour in the top row of **Figure 25**. The Fermi contours of the LAO overlayer are more complicated. First, the spherical Fermi contour that is formed by the Ti d states from the interfacial TiO_2 layer dominates around the Γ point; although the LaO interfacial layer contributes insignificantly, this is a result of hybridization. Second, a rhombic Fermi spot appears at Γ attributed to the d-states of interfacial Ti and another Ti in the adjacent TiO_2 layer. There are rather narrow Fermi arms along the [10] directions that stem from the two TiO_2 layers and which make the Fermi texture weakly anisotropic.

The doped LAO surface yields additional contributions to the Fermi contours; refer to the bottom panels of Figure 25 for the $AlO_{1.9}$ surface, especially the sizable weights associated with the ellipses centered at Γ and elongated along [10]. These contours are formed by Ti d states from the second and interfacial layers of STO. This finding suggests that the anisotropy of the conductivity may be enhanced in case of O vacancies.

The presence of an open surface spreads the 2DEG spatially, as also shown in Figure 19. Consequently, the two Fermi cross
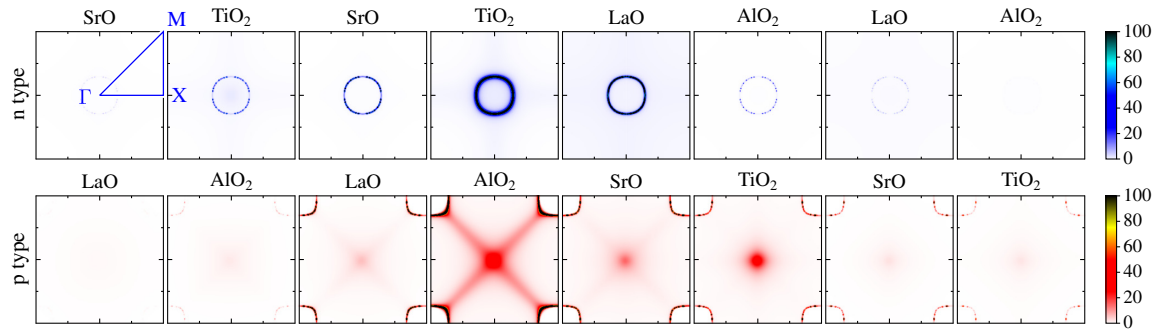
Figure 23. (001) cross sections of the Bloch spectral function projected on each atomic layer of LAO/STO(001) near its *n* (upper panels) and *p* (lower panels) interfaces.
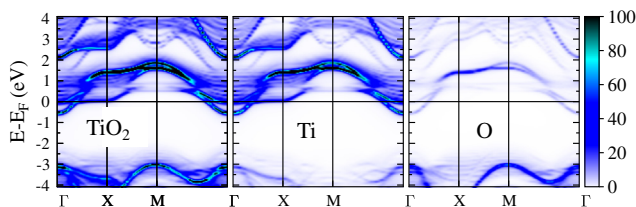

Figure 24. Bloch spectral function of a LAO/STO(001) overlayer projected onto interfacial Ti along high-symmetry directions of the 2D Brillouin zone. (Motivated by Maznichenko et al.[45])

sections (a spot and arms) which appear in addition to the spherical contour may increase the variety of the effective electron masses associated with the 2DEG. When the surface layer contains O vacancies, the Fermi contour becomes even more complicated and anisotropic, as shown in the bottom row of Figure 25. We anticipate that the effective electron mass may range between $0.4\,m_e$ and $0.6\,m_e$, which agrees with the data measured so far.[38,60,61]

5. Conclusions

The 2DEG at the (001) interface between two robustly insulating ABO_3 perovskites was modeled from first principles using the efficient GF method within standard DFT. The 2D effect was evaluated by calculating its charged density for various polar/nonpolar and perfect LAO/STO(001), LFO/STO(001), and STO/KTO(001) superlattices. We illustrated a necessary condition for a 2DEG: at least one side of the (001) perovskite interface has to be polar, whereas the material-dependent interfacial band bending determines the 2DEG's carrier density and its transport properties. Our calculations for the ideal polar/polar interfaces, such as $LaAlO_3/KTaO_3(001)$, and also for the (110) and (111) interfaces of LAO/STO suggest that this scenario may not enhance the 2DEG density. Therefore, polar overlayers of LAO or LFO grown on a STO(001) substrate which form unavoidably an n-type TiO_2/LaO interface represent suitable materials for hosting a 2DEG.

Focusing on LAO/STO(001) interfaces, we simulated the 2DEG and its possible enhancement for a slab geometry with
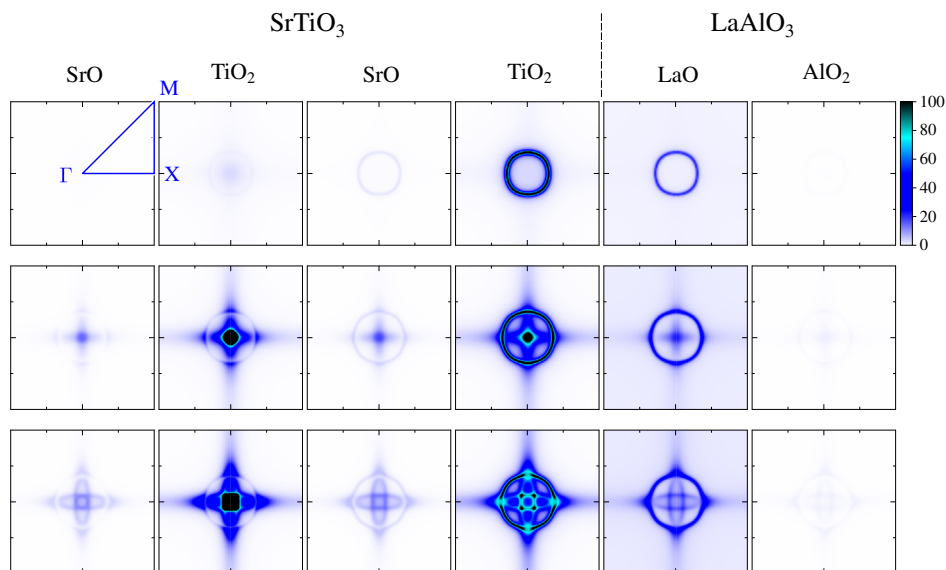

Figure 25. (001) cross sections of the Bloch spectral function projected on selected atomic layers near the n-type interface of LAO/STO. The top and center row are for a perfect heterostructure and a perfect surface layer AlO_2, respectively. The bottom row shows results calculated for the $AlO_{1.9}$ surface with O vacancies. (Motivated by Maznichenko et al.[45])

vacuum. We show how the degree of oxidation at the AlO_2-terminated LAO surface changes the 2DEG's density at the buried n interface. This model mimics to some extent ionic liquid gating, that is, the technique that has been used for LAO/STO and LAO/LFO. The degree of doping below and above the AlO_2 surface composition was simulated using the GF method and CPA. For the ideal LAO surface, we demonstrate that the 2DEG density, which emerges at the buried interface, becomes more pronounced as compared to that of the corresponding superlattice. Moreover, we anticipate that the 2DEG density can be enhanced and controlled by the presence of surplus oxygen atoms or oxygen vacancies at the LAO surface. From the Fermi contours that appear due to the 2DEG, we conclude that the LAO surface affects transport-related properties of LAO/STO(001). In fact, two weakly anisotropic transport channels are added to the former highly isotropic spherical Fermi contour that enhances the electron effective mass in the range of $0.4\,m_e$–$0.6\,m_e$.

In a next step, it is worthwhile to study the Rashba effect and the spin polarization of the 2DEG carriers.[62] We believe that our findings presented in this work may stimulate further experimental and theoretical studies of the effect of liquid gating in LAO/STO and similar interfaces with a polar discontinuity.

Acknowledgements

Conflict of Interest

The authors declare no conflict of interest.

Keywords

[1] A. Ohtomo, H. Y. Hwang, *Nature* **2004**, *427*, 423.
[2] S. Thiel, G. Hammerl, A. Schmehl, C. W. Schneider, J. Mannhart, *Science* **2006**, *313*, 1942.
[3] N. Nakagawa, H. Y. Hwang, D. A. Muller, *Nat. Mater.* **2006**, *5*, 204.
[4] H. Y. Hwang, Y. Iwasa, M. Kawasaki, B. Keimer, N. Nagaosa, Y. Tokura, *Nat. Mater.* **2012**, *11*, 103.
[5] S. Stemmer, S. J. Allen, *Annu. Rev. Mater. Res.* **2014**, *44*, 151.
[6] G. Singh-Bhalla, C. Bell, J. Ravichandran, W. Siemons, Y. Hikita, S. Salahuddin, A. F. Hebard, H. Y. Hwang, R. Ramesh, *Nat. Phys.* **2010**, *7*, 80.
[7] M. Lorenz, M. S. R. Rao, T. Venkatesan, E. Fortunato, P. Barquinha, R. Branquinho, D. Salgueiro, R. Martins, E. Carlos, A. Liu, F. K. Shan, M. Grundmann, H. Boschker, J. Mukherjee, M. Priyadarshini, N. DasGupta, D. J. Rogers, F. H. Teherani, E. V. Sandana, P. Bove, K. Rietwyk, A. Zaban, A. Veziridis, A. Weidenkaff, M. Muralidhar, M. Murakami, S. Abel, J. Fompeyrine, J. Zuniga-Perez, R. Ramesh, et al., *J. Phys. D Appl. Phys.* **2016**, *49*, 433001.
[8] J. Goniakowski, F. Finocchi, C. Noguera, *Rep. Prog. Phys.* **2008**, *71*, 016501.
[9] C. Noguera, J. Goniakowski, *Chem. Rev.* **2013**, *113*, 4073.
[10] N. C. Bristowe, P. Ghosez, P. B. Littlewood, E. Artacho, *J. Phys. Condens. Matter* **2014**, *26*, 143201.
[11] C. Nougera, J. Goniakowski, *Oxide Materials at the Two-Dimensional Limit*, Springer Series in Materials Science, Vol. 234, Springer, Cham, Switzerland **2016**, p. 201.
[12] P. Xu, W. Han, P. M. Rice, J. Jeong, M. G. Samant, K. Mohseni, H. L. Meyerheim, S. Ostanin, I. V. Maznichenko, I. Mertig, E. K. U. Gross, A. Ernst, S. S. P. Parkin, *Adv. Mater.* **2017**, *29*, 1604447.
[13] C. Li, Z. Liu, W. Lü, X. R. Wang, A. Annadi, Z. Huang, S. Zeng, T. Venkatesan, *Sci. Rep.* **2015**, *5*, 13314.
[14] M. Huijben, G. Rijnders, D. H. A. Blank, S. Bals, S. V. Aert, J. Verbeeck, G. V. Tendeloo, A. Brinkman, H. Hilgenkamp, *Nat. Mater.* **2006**, *5*, 556.
[15] F. Zhang, P. Lv, Y. Zhang, S. Huang, C. M. Wong, H. M. Yau, X. Chen, Z. Wen, X. Jiang, C. Zeng, J. Hong, J. y. Dai, *Phys. Rev. Lett.* **2019**, *122*, 257601.
[16] Z. Gao, X. Huang, P. Li, L. Wang, L. Wei, W. Zhang, H. Guo, *Adv. Mater. Interfaces* **2018**, *5*, 1701565.
[17] H. L. Meyerheim, F. Klimenta, A. Ernst, K. Mohseni, S. Ostanin, M. Fechner, S. Parihar, I. V. Maznichenko, I. Mertig, J. Kirschner, *Phys. Rev. Lett.* **2011**, *106*, 087203.
[18] J. Ye, S. Inoue, K. Kobayashi, Y. Kasahara, H. Yuan, H. Shimotani, Y. Iwasa, *Nat. Mater.* **2010**, *9*, 125.
[19] S. Zeng, W. Lü, Z. Huang, Z. Liu, K. Han, K. Gopinadhan, C. Li, R. Guo, W. Zhou, H. H. Ma, L. Jian, T. Venkatesan, *ACS Nano* **2016**, *10*, 4532.
[20] S. W. Zeng, X. M. Yin, T. S. Herng, K. Han, Z. Huang, L. C. Zhang, C. J. Li, W. X. Zhou, D. Y. Wan, P. Yang, J. Ding, A. T. S. Wee, J. M. D. Coey, T. Venkatesan, A. Rusydi, A. Ariando, *Phys. Rev. Lett.* **2018**, *121*, 146802.
[21] E. Maniv, Y. Dagan, M. Goldstein, *MRS Adv.* **2017**, *2*, 1243.
[22] I. Pallecchi, F. Telesio, D. Li, A. Fête, S. Gariglio, J. M. Triscone, A. Filippetti, P. Delugas, V. Fiorentini, D. Marré, *Nat. Commun.* **2015**, *6*, 6678.
[23] P. Gallagher, M. Lee, T. A. Petach, S. W. Stanwyck, J. R. Williams, K. Watanabe, T. Taniguchi, D. Goldhaber-Gordon, *Nat. Commun.* **2015**, *6*, 6437.
[24] W. Liu, S. Gariglio, A. Fête, D. Li, M. Boselli, D. Stornaiuolo, J. M. Triscone, *APL Mater.* **2015**, *3*, 062805.
[25] L. Qiao, T. C. Droubay, V. Shutthanandan, Z. Zhu, P. V. Sushko, S. A. Chambers, *J. Phys. Condens. Matter* **2010**, *22*, 312201.
[26] L. Qiao, T. Droubay, T. Kaspar, P. Sushko, S. Chambers, *Surf. Sci.* **2011**, *605*, 1381.
[27] N. Pavlenko, T. Kopp, E. Y. Tsymbal, J. Mannhart, G. A. Sawatzky, *Phys. Rev. B* **2012**, *86*, 064431.
[28] V. Vonk, J. Huijben, D. Kukuruznyak, A. Stierle, H. Hilgenkamp, A. Brinkman, S. Harkema, *Phys. Rev. B* **2012**, *85*, 045401.
[29] R. Pentcheva, W. E. Pickett, *Phys. Rev. Lett.* **2009**, *102*, 107602.
[30] R. Pentcheva, W. E. Pickett, *J. Phys. Condens. Matter* **2010**, *22*, 043001.
[31] M. S. Park, S. H. Rhim, A. J. Freeman, *Phys. Rev. B* **2006**, *74*, 205416.
[32] K. Janicka, J. P. Velev, E. Y. Tsymbal, *Phys. Rev. Lett.* **2009**, *102*, 106803.
[33] M. Breitschaft, V. Tinkl, N. Pavlenko, S. Paetel, C. Richter, J. R. Kirtley, Y. C. Liao, G. Hammerl, V. Eyert, T. Kopp, J. Mannhart, *Phys. Rev. B* **2010**, *81*, 153414.
[34] P. R. Willmott, S. A. Pauli, R. Herger, C. M. Schlepütz, D. Martoccia, B. D. Patterson, B. Delley, R. Clarke, D. Kumah, C. Cionca, Y. Yacoby, *Phys. Rev. Lett.* **2007**, *99*, 155502.

[35] A. Janotti, L. Bjaalie, L. Gordon, C. G. Van de Walle, *Phys. Rev. B* **2012**, *86*, 241108.

[36] L. Yu, A. Zunger, *Nat. Commun.* **2014**, *5*, 5118.

[37] M. A. Islam, D. Saldana-Greco, Z. Gu, F. Wang, E. Breckenfeld, Q. Lei, R. Xu, C. J. Hawley, X. X. Xi, L. W. Martin, A. M. Rappe, J. E. Spanier, *Nano Lett.* **2016**, *16*, 681.

[38] H. Guo, W. A. Saidi, J. Zhao, *Phys. Chem. Chem. Phys.* **2016**, *18*, 28474.

[39] H. L. Zhuang, L. Zhang, H. Xu, P. Kent, P. Ganesh, V. R. Cooper, *Sci. Rep.* **2016**, *6*, 25452.

[40] D. Doennig, R. Pentcheva, *Sci. Rep.* **2015**, *5*, 7909.

[41] R. Pentcheva, W. E. Pickett, *Phys. Rev. B* **2006**, *74*, 035112.

[42] M. Lüders, A. Ernst, W. M. Temmerman, Z. Szotek, P. J. Durham, *J. Phys. Condens. Matter* **2001**, *13*, 8587.

[43] H. Ebert, D. Koedderitzsch, J. Minar, *Rep. Prog. Phys.* **2011**, *74*, 096501.

[44] I. Maznichenko, S. Ostanin, V. Dugaev, I. Mertig, A. Ernst, *Phys. Rev. Mater.* **2018**, *2*, 074003.

[45] I. Maznichenko, S. Ostanin, A. Ernst, I. Mertig, *Phys. Rev. Mater.* **2019**, *3*, 074006.

[46] B. L. Gyorffy, *Phys. Rev. B* **1972**, *5*, 2382.

[47] V. Borisov, S. Ostanin, I. Mertig, *Phys. Chem. Chem. Phys.* **2015**, *17*, 12812.

[48] K. D. Fredrickson, A. A. Demkov, *Phys. Rev. B* **2015**, *91*, 115126.

[49] R. Pentcheva, M. Huijben, K. Otte, W. E. Pickett, J. E. Kleibeuker, J. Huijben, H. Boschker, D. Kockmann, W. Siemons, G. Koster, H. J. W. Zandvliet, G. Rijnders, D. H. A. Blank, H. Hilgenkamp, A. Brinkman, *Phys. Rev. Lett.* **2010**, *104*, 166804.

[50] H. Chen, A. Kolpak, S. Ismail-Beigi, *Phys. Rev. B* **2010**, *82*, 085430.

[51] A. F. Santander-Syro, C. Bareille, F. Fortuna, O. Copie, M. Gabay, F. Bertran, A. Taleb-Ibrahimi, P. Le Fèvre, G. Herranz, N. Reyren, M. Bibes, A. Barthélémy, P. Lecoeur, J. Guevara, M. J. Rozenberg, *Phys. Rev. B* **2012**, *86*, 121107.

[52] H. Lee, N. Campbell, J. Lee, T. J. Asel, T. R. Paudel, H. Zhou, J. W. Lee, B. Noesges, J. Seo, B. Park, L. J. Brillson, S. H. Oh, E. Y. Tsymbal, M. S. Rzchowski, C. B. Eom, *Nat. Mater.* **2018**, *17*, 231.

[53] C. P. Su, A. K. Singh, T. C. Wu, M. C. Chen, Y. C. Lai, W. L. Lee, G. Y. Guo, M. W. Chu, *Phys. Rev. Mater.* **2019**, *3*, 075003.

[54] A. Annadi, Q. Zhang, X. Renshaw Wang, N. Tuzla, K. Gopinadhan, W. M. Lü, A. Roy Barman, Z. Q. Liu, A. Srivastava, S. Saha, Y. L. Zhao, S. W. Zeng, S. Dhar, E. Olsson, B. Gu, S. Yunoki, S. Maekawa, H. Hilgenkamp, T. Venkatesan, *Nat. Commun.* **2013**, *4*, 1838.

[55] G. Herranz, F. Sánchez, N. Dix, M. Scigaj, J. Fontcuberta, *Sci. Rep.* **2012**, *2*, 758.

[56] S. Davis, V. Chandrasekhar, Z. Huang, K. Han, Ariando, T. Venkatesan, *Phys. Rev. B* **2017**, *95*, 035127.

[57] M. P. Warusawithana, C. Richter, J. A. Mundy, P. Roy, J. Ludwig, S. Paetel, T. Heeg, A. A. Pawlicki, L. F. Kourkoutis, M. Zheng, M. Lee, B. Mulcahy, W. Zander, Y. Zhu, J. Schubert, J. N. Eckstein, D. A. Muller, C. S. Hellberg, J. Mannhart, D. G. Schlom, *Nat. Commun.* **2013**, *4*, 2351.

[58] M. Fechner, S. Ostanin, I. Mertig, *Phys. Rev. B* **2008**, *77*, 094112.

[59] H. Meyerheim, F. Klimenta, A. Ernst, K. Mohseni, S. Ostanin, M. Fechner, S. Parihar, I. Maznichenko, I. Mertig, J. Kirschner, *Phys. Rev. Lett.* **2011**, *106*, 087203.

[60] Z. Zhong, A. Tóth, K. Held, *Phys. Rev. B* **2013**, *87*, 161102.

[61] A. McCollam, S. Wenderich, M. K. Kruize, V. K. Guduru, H. J. A. Molegraaf, M. Huijben, G. Koster, D. H. A. Blank, G. Rijnders, A. Brinkman, H. Hilgenkamp, U. Zeitler, J. C. Maan, *APL Mater.* **2014**, *2*, 022102.

[62] C. Bhandari, S. Satpathy, *Phys. Rev. B* **2018**, *98*, 041303.